HHS Public Access

Author manuscript

Nat Neurosci. Author manuscript; available in PMC 2019 October 08.

Published in final edited form as:

Nat Neurosci. 2019 May ; 22(5): 820–827. doi:10.1038/s41593-019-0371-x.

Working memory revived in older adults by synchronizing rhythmic brain circuits

Robert M. G. Reinhart[*] and **John A. Nguyen**

Department of Psychological & Brain Sciences, Center for Systems Neuroscience, Cognitive Neuroimaging Center, Center for Research in Sensory Communications and Neural Technology, Boston University, Boston, MA 02215, USA.

Abstract

Understanding normal brain aging and developing methods to maintain or improve cognition in older adults are major goals of fundamental and translational neuroscience. Here, we show a core feature of cognitive decline - working memory deficits - emerges from disconnected local and long-range circuits instantiated by theta-gamma phase-amplitude codes in temporal cortex and theta phase synchronization across frontotemporal cortex. We developed a noninvasive stimulation procedure for modulating long-range theta interactions in adults aged 60–76 years. After 25 minutes of stimulation, frequency tuned to individual brain network dynamics, we observed a preferential increase in neural synchronization patterns and the return of sender-receiver relationships of information flow within and between frontotemporal regions. The end result was rapid improvement in working memory performance that outlasted a 50-minute post-stimulation period. The results provide insight into the physiological foundations of age-related cognitive impairment and contribute groundwork for future non-pharmacological interventions targeting aspects of cognitive decline.

Over the last century, we have witnessed an astonishing rise in the prevalence of cognitive decline and dementia in older adults [1, 2], which is expected to grow even faster in coming decades as the global population rapidly ages [2, 3]. Deficits in working memory - the ability to actively store behaviorally useful information "in mind" over a period of seconds - play a central role in normal neurocognitive aging and the rapid cognitive deterioration associated with dementias, such as Alzheimer's disease [4, 5]. The underlying cause of age differences in working memory and other cognitive impairment has been hypothesized to partly derive

[*]Correspondence to: Robert M. G. Reinhart, 677 Beacon St., Rm 312, Boston, MA 02215, rmgr@bu.edu.

Author contributions

R.M.G.R. conceived the experiments. R.M.G.R. and J.A.N. conducted the experiments and analyzed the data. R.M.G.R. wrote the paper.

Competing interests

The authors declare no competing interests.

Code availability

All code used in this study can be obtained by contacting the corresponding author.

Data availability

The data that support the findings of this study are available from the corresponding author upon request.

from a variety of neurobiological sources, such as changes in grey matter volume and white matter integrity, global and regional cerebral blood flow, neurotransmitter binding potential and receptor density, and more recently, the functional connectivity of large-scale brain networks [4, 6]. Accumulating evidence suggests that age-related memory and cognitive decline is associated with alterations in the relationships between different brain areas [7, 8], potentially due to anatomical and functional dysconnectivity between brain areas that normally function in a coordinated or synchronous fashion [9, 10].

Current theories in neuroscience propose that cross-frequency coupling and phase synchronization may index neural interactions of information gating and communication within and between broad networks during cognition [11, 12]. Cross-frequency coupling has been proposed to constitute a flexible mechanism for combining information across different temporal scales within local cortical networks [13, 14]. During working memory maintenance, a specific form of cross-frequency coupling called theta (4–8 Hz) gamma (>25 Hz) phase-amplitude coupling (PAC), in which the amplitude of gamma rhythms is coupled to the phase of theta rhythms, has been observed in temporal cortex [14, 15], and is thought to reflect the local processing and storage of memory contents [12, 16]. In contrast, phase synchronization among task-relevant areas may integrate information across multiple spatial scales [17]. Phase synchronization, particularly in the upper theta frequency band, has been seen between prefrontal and temporal areas [14, 18], and is hypothesized to reflect a mechanism by which prefrontal cortex interacts with sensory areas to control and monitor resources for content processing and storage in working memory [19, 20].

Recently, transcranial alternating-current stimulation (tACS), when paired with electroencephalographic (EEG) measures of functional connectivity, has shown great promise in preferentially modulating rhythmic cortical networks in a causal, frequency-specific, and sometimes bidirectional manner, with lasting behavioral effects [21–23]. In addition, mounting evidence from tACS behavioral studies suggest it may be possible to influence working memory processing and capacity by targeting cortical regions with tACS in the theta frequency band [24, 25].

Here, we used electrophysiological measurements of PAC and phase synchronization to evaluate the claim that working memory cognitive decline derives from the inefficient orchestration of rhythmic neuronal activity within large-scale cortical networks. We predict that if theta-gamma PAC in temporal areas and theta phase synchronization between prefrontal and temporal areas underlies successful working memory maintenance in younger adults, then older adults with deficits in working memory, whose brain circuits we hypothesize are uncoupled or disconnected, should lack or exhibit deficiencies in these neural coding schemes. Further, we develop a tACS protocol that targets prefrontal and temporal regions, simultaneously, with the goal of augmenting the putative signatures of maintenance-related functional connectivity (i.e., PAC and phase synchronization) and improving working memory performance for older adults. We predict that a “synchronizing” or inphase tACS protocol that can bias frontotemporal network connectivity may facilitate the neural integration indexed by theta-gamma PAC and theta phase synchronization, and thereby boost working memory performance for older adults.

To test these predictions, we conducted a double blind, sham-controlled, within-subjects experiment using EEG and high-definition tACS (HD-tACS) (i.e., a form of tACS that provides more precise targeting of cortical structures) (Fig. 1a, see Methods). In Experiment 1, younger adults participated in the sham day, while older adults participated in sham and active stimulation days. HD-tACS was applied for 25 minutes while subjects performed 10 blocks of a change-detection task with images of real-world objects (Fig. 1b). After stimulation, subjects continued to perform the task for another 20 blocks. In what follows, first we report the effects of age on measures of neural synchronization and behavior using data from the sham conditions of each age group. Then, we examine the impact of HD-tACS on neural synchronization and behavior in older adults using data from their sham and active stimulation conditions. Finally, we report the results from a series of follow-up experiments, which sought to replicate and extend the principal behavioral findings of Experiment 1.

Results

Working memory performance is impaired in older adults

Age negatively impacted working memory performance. First, we collapsed data across post-stimulation memory blocks of the sham condition and found that older adults were markedly slower and less accurate at performing the task as compared with younger adults (Fig. 2a). No response biases were observed between age groups ($t_{82} = 1.074$, $p = 0.286$, $d_z = 0.234$). Next, we examined the evolution and dynamics of behavior throughout the stimulation and post-stimulation periods by sorting the data from memory blocks into nine sequential 4-minute-long bins across the 75-minute recording period of the experiment (Fig. 2b, c). Both age groups showed gradual performance decline with increasing time on the task (older accuracy, $F_{8,328} = 5.001$, $p = 0.009$, partial $\eta^2 = 0.109$; older RT, $F_{8,328} = 4.859$, $p = 0.005$, partial $\eta^2 = 0.106$; younger accuracy, $F_{8,328} = 3.059$, $p = 0.035$, partial $\eta^2 = 0.069$; younger RT, $F_{8,328} = 6.431$, $p < 0.01$, partial $\eta^2 = 0.136$). However, no group x time interactions reached significance (accuracy, $F_{8,656} = 1.418$, $p = 0.236$, partial $\eta^2 = 0.017$; RT, $F_{8,656} = 2.055$, $p = 0.102$, partial $\eta^2 = 0.024$), suggesting that performance decline, likely due to waning attention and increased fatigue, was comparable across age groups. Performance differences between age groups were significant at every sequential time bin for accuracy and RT, indicating that age-related impairments in working memory were stable and endured throughout the length of the recording. The results conform to previous research [4–6, 26], and suggest that older adults struggled to maintain robust representations of task-relevant information in working memory.

Theta-gamma rhythms are uncoupled in older adults during working memory maintenance

To test whether age differences in working memory resulted from a lack of temporal integration within large-scale cortical networks, we computed PAC at all electrodes for different combinations of low (2–16 Hz) and high (18–120 Hz) frequencies during the memory maintenance period of the task (500 to 3000 ms post-target onset), and used cluster permutation statistics to identify clusters of electrodes and frequencies showing significant differences in PAC between memory and control blocks for each age group. Figure 3a shows the results. For older adults, no significant clusters in electrode or source space emerged as significant. In contrast, for younger adults, one cluster of left temporal electrodes showed

significantly increased memory-specific PAC ($p_{corrected} < 0.01$) between 7–9 Hz phase frequencies and 26–34 Hz amplitude frequencies. In source space, cluster analysis estimated this PAC effect to the left temporal cortex. Further, a group x block interaction was significant for PAC at the 8-Hz to 30-Hz center frequencies collapsed across left temporal electrodes ($p_{corrected} < 0.01$; Fig. 3b), demonstrating frequency specificity of the PAC deficiency older adults experienced on memory trials.

To provide an alternative means of evaluating this nested cortical network in younger adults and its potentially disconnected nature in older adults, we explored the phase-angle preference and information flow direction of memory-related theta-gamma PAC within left temporal electrodes across subjects. Unlike younger adults who showed intact working memory network nesting on memory trials, evidenced by significantly nonuniform theta phase sorted gamma amplitude values ($z = -2.724$, $p = 0.003$), older adults had sorted amplitude values that did not differ significantly from a random distribution ($z = -0.540$, $p = 0.286$) (Fig. 3c). Analysis of PAC directionality using phase-slope index (PSI) corroborated this pattern of results. Younger adults showed theta phase predictive of gamma amplitude over left temporal electrodes, rather than the converse ($t_{41} = 3.029$, $p = 0.004$, $d_z = 0.467$), but this directionality was markedly reduced for older adults relative to younger subjects ($t_{82} = 2.735$, $p = 0.009$, $d_z = 0.422$) (Fig. 3d).

To provide more detailed information on the relationships between PAC and behavior, we performed regression analyses at the individual subject level. As shown in Figure 3e, younger adults with stronger theta-gamma PAC performed the task with higher accuracy, relative to individuals with weaker coupling ($r_{41} = 0.611$, $p < 0.01$). In contrast, older adults showed no significant relationship between performance accuracy and theta-gamma PAC collapsed across left temporal electrodes ($r_{41} = 0.188$, $p = 0.233$). The results suggest that theta-gamma PAC in younger adults is behaviorally significant, predictive of subsequent working memory success. However, when theta-gamma rhythms become largely uncoupled, as in the brains of older people, PAC appears to lose its behavioral usefulness in driving cognitive performance.

Long-range theta synchronization is compromised in older adults but short-range gamma synchronization is intact

We found differential effects of age on theta and gamma phase dynamics during working memory maintenance. We computed phase-locking value (PLV) from seed voxels in left temporal cortex to all other voxels in the brain in the theta band revealed by PAC (7–9 Hz). After correcting for multiple comparisons, the prefrontal cortex showed significant increased phase synchronization with left temporal cortex during memory maintenance compared to the non-memory control block ($p_{corrected} < 0.01$; Fig. 4a). However, this effect was only significant for younger adults. Older subjects exhibited no frontotemporal theta synchronization and their memory-specific PLV was significantly reduced relative to younger adults (Fig. 4a). In contrast, the same temporal cortex seeded connectivity analysis in the gamma band revealed a different pattern of results. A significant cluster ($p_{corrected} < 0.01$) of memory-related gamma PLV was detected in nearby regions (e.g., lateral occipital cortex) for both age groups, and did not differ across groups (Fig. 4b). Directionality

analysis provided complementary support for these findings. Results from the theta band suggested prefrontal cortex was the sender and temporal cortex was the receiver for younger adults ($t_{41} = -2.959$, $p = 0.005$, $d_z = 0.457$). However, PSIs in older adults did not reach significance ($t_{41} = -0.382$, $p = 0.705$, $d_z = 0.059$). In contrast, no preferred direction in the flow of information between temporal and occipital regions was apparent in the gamma band for either age group ($ts_{41} < 1.489$, $ps > 0.144$, $ds_z < 0.230$). The results suggest a preferential impact of age on maintenance-related neural connectivity, whereby local communication among sensory areas indexed by short-range occipitotemporal gamma synchronization appears intact in older age, but global communication directed by prefrontal cortex indexed by long-range frontotemporal theta synchronization appears disconnected or insufficiently active in older compared to younger people.

HD-tACS improves working memory in older adults in a stable and enduring manner

HD-tACS appeared to eliminate age-related impairment in working memory accuracy. After 25 minutes of stimulation, older adults showed a significant increase in task accuracy relative to sham (Fig. 2a), without changing response bias ($t_{41} = 0.770$, $p = 0.446$, $d_z = 0.119$). This behavioral improvement was sufficient to remove the original group difference in working memory accuracy, as older adults after stimulation exhibited a mean accuracy level statistically indistinguishable from that of younger adults at baseline. Further, stimulation had a preferential impact across behavioral metrics. While performance accuracy was boosted following stimulation, we observed no change in mean RT across conditions (Fig. 2a). This suggests that the stimulation-induced benefit in behavioral success was not merely due to subjects trading speed for accuracy between the different stimulation conditions.

A finer-grained analysis of within-session behavioral dynamics revealed that the stimulation-induced improvement in accuracy occurred relatively quickly, within approximately 12 minutes of HD-tACS delivery, and continued over the full 50-minute duration of post-stimulation blocks (Fig. 2b). During the first 4 minutes of stimulation no differences in performance accuracy between sham and active conditions were apparent. However, by time bin 2 (i.e., between 8–12 minutes from the start of stimulation) older adults began to show significant accuracy gains, which peaked by the first time bin of the post-stimulation period (i.e., time bin 4), and continued for the duration of the experiment. Stimulation-induced changes in RT lagged behind those in accuracy, and were short-lived (Fig. 2c). Significant RT speeding was first observed towards the end of the stimulation period (i.e., time bin 3), and then again offline only at time bins 4 and 6. The stimulation x time interactions on accuracy ($F_{8,656} = 16.707$, $p < 0.01$, partial $\eta^2 = 0.169$) and RT ($F_{8,656} = 3.655$, $p = 0.009$, partial $\eta^2 = 0.043$) were significant. The results suggest that stimulation rapidly improved task accuracy in older adults with lasting and stable offline effects that continued for the length of the experiment, whereas stimulation effects on performance speed were more variable and fleeting.

HD-tACS reinstates theta-gamma coupling and its behavioral relevance in older adults

After stimulation, we observed a preferential increase in local theta-gamma PAC, paralleling the improvement in behavioral accuracy in older adults. This was evidenced by a number of

findings following active HD-tACS. First, we identified a cluster of left temporal electrodes showing significantly increased PAC ($p_{corrected} < 0.01$; Fig. 3a) between 7–9 Hz phase and 26–34 Hz amplitude frequencies in the memory relative to non-memory control block. Computing PAC in source space produced a similar result in left temporal cortex. Second, the stimulation x block interaction nearest the 8-Hz phase 30-Hz amplitude center frequencies from left temporal electrodes was significant ($p_{corrected} < 0.01$; Fig. 3b). Third, older subjects now exhibited significantly nonuniform theta sorted gamma amplitude values ($z = -2.041$, $p = 0.024$; Fig. 3c). Fourth, theta phase was predictive of gamma amplitude over left temporal electrodes, rather than the opposite ($t_{41} = 2.235$, $p = 0.031$, $d_z = 0.345$; Fig. 3d). Fifth, after stimulation had restructured theta-gamma PAC in older adults, the strength of this coupling was now significantly predictive of individual working memory accuracy ($r_{41} = 0.571$, $p < 0.01$; Fig. 3e). The results suggest that it may be possible to improve working memory function for older adults by using a noninvasive manipulation of the brain that appears to re-establish the nesting of a cortical network in temporal cortex indexed by cross-frequency PAC.

HD-tACS enhances theta, but not gamma, phase synchronization in older adults

HD-tACS exerted a preferential influence on maintenance-related frontotemporal theta phase synchronization in older adults. As illustrated in Figure 4a, after stimulation, a significant cluster ($p_{corrected} < 0.01$) in prefrontal cortex showed increased PLV with left temporal cortex during memory relative to control blocks, whereas the same subjects in the sham condition generated no significant clusters of temporal-seeded PLV in the theta band. This resulted in a significant difference in memory-specific theta PLV between active and sham conditions for older adults (Fig. 4a). Further, the expected information flow direction between prefrontal and temporal regions was effectively reinstated ($t_{41} = -2.592$, $p = 0.013$, $d_z = 0.400$). Repeating the seeded PLV analysis for the gamma band yielded a significant cluster ($p_{corrected} < 0.01$) of memory-related gamma in regions nearest lateral occipital cortex for older adults during both sham and active stimulation conditions (Fig. 4b). This resulted in no significant difference in memory-specific gamma PLV across conditions (Fig. 4b). Both stimulation conditions showed no preferred direction of information flow among occipitotemporal gamma synchronization ($ts_{41} < -1.221$, $ps > 0.229$, $ds_z > 0.188$). The results suggest occipitotemporal gamma connectivity in older adults was neither impaired at baseline, nor modulated by HD-tACS. It is possible that age-related preservation of occipitotemporal gamma plays a role in compensating for disconnected frontal control systems. Moreover, the preferential modulation of theta, but not gamma, synchronization by HD-tACS highlights the frequency specificity of this procedure, allowing us to potentially manipulate activity along a particular frequency channel of neural communication.

Ruling out potential confounds

We ran several analyses to confirm the validity of the main findings. First, we assessed spectral power. It is possible that the effects of age or stimulation altered spectral power in the same frequencies and electrodes or voxels involved in PAC, thereby changing signal-to-noise ratio and phase estimation quality. However, we found no significant changes in baseline-corrected mean power values across the delay period (500 to 3000 ms post-target onset) between blocks for either age group or stimulation condition (7–9 Hz electrodes, ts_{41}

< 1.334, ps > 0.189, ds_z < 0.206; 7–9 Hz voxels, ts_{41} < 1.090, ps > 0.282, ds_z < 0.168; 26–34 Hz electrodes, ts_{41} < 0.849, ps > 0.401, ds_z < 0.131; 26–34 Hz voxels, ts_{41} < 0.999, ps > 0.324, ds_z < 0.154). Further, there were no significant changes in signal-to-noise ratios in memory-related EEG at the frequencies, electrodes, or voxels involved in PAC between age groups or stimulation conditions (ts_{41} < 1.325, ps > 0.193, ds_z < 0.204). Of note, while age-related rotations in 1/f spectra have been previously observed in parietal and central midline regions during maintenance of lateralized colored squares [27], studies are needed to examine the presence and spatial topography of age and neural noise correlations during working memory tasks that use complex real-world objects engaging frontotemporal regions and stimulus controls that account for vigilance and attention effects to better isolate maintenance-related neural activity. Additionally, we tested for power modulations in the theta band at both temporal seed and prefrontal cluster locations used for measuring seeded PLV. We found no significant results in either group or stimulation condition (seed, ts_{41} < −1.394, ps > 0.171, ds_z < 0.215; cluster, ts_{41} < 0.734, ps > 0.467, ds_z < 0.113). Finally, we examined whether PAC results relied on the non-sinusoidal waveform shape of the low-frequency rhythm [28], by measuring phase-phase coupling (PPC) [29]. We tested for significant differences in PPC within the cluster of electrodes showing enhanced memory-related theta-gamma PAC. A two-tailed paired t-test on the mean across left temporal electrodes included in the PAC cluster produced no significant differences in PPC between blocks for either age group (ts_{41} < 0.754, ps > 0.455, ds_z < 0.116) or stimulation condition (ts_{41} < 1.364, ps > 0.180, ds_z < 0.210) (see Supplementary Fig. 1 for additional control analyses).

HD-tACS improvement requires precise spatiospectral targeting of the brain

In Experiment 2, we sought to replicate the principal behavioral findings in a new cohort of older adults and examine the frequency and anatomical specificity of HD-tACS by using nontuned stimulation and montages that targeted frontal and temporal regions, separately (see Methods; Figs 1a, 5a, b). There were four main findings (Fig. 6). First, during post-stimulation memory blocks of the sham condition, performance was impaired in the new group of older adults compared to the 20-year-olds from Experiment 1 (RT, t_{68} = 2.173, p = 0.033, d_z = 0.519; accuracy, t_{68} = 4.186, p < 0.01, d_z = 1.001), and these impairments were observed at all nine sequential 4-minute-long time bins over the full duration of the experiment, including stimulation and post-stimulation periods (RT, ts_{68} > 2.546, ps < 0.014, ds_z > 0.609; accuracy, ts_{68} > 3.332, ps < 0.01, ds_z > 0.797), replicating the between-group differences of Experiment 1. Second, frontotemporal theta-tuned stimulation relative to sham preferentially enhanced the accuracy of working memory behavior in older adults independent of RT, and these post-stimulation accuracy gains were large enough to eliminate age-related differences in behavior between groups (t_{68} = 0.956, p = 0.343, d_z = 0.229), consistent with results from Experiment 1. Moreover, like Experiment 1, the stimulation-induced accuracy improvements remained significantly elevated relative to sham levels for the entire experiment beginning with time bin 2 (ts_{27} > 2.886, ps < 0.008, ds_z > 0.545), whereas RT speeding lagged behind accuracy gains and were short-lived, only observed at time bins 3–5 (ts_{27} > 2.537, ps < 0.017, ds_z > 0.479). Third, although the frontotemporal 8-Hz nontuned stimulation appeared to have a slight beneficial influence, qualitatively, on performance accuracy in post-stimulation blocks, neither accuracy, nor RT significantly differed compared to sham. Similarly, no differences between sham and 8-Hz conditions at

any of the nine sequential 4-minute-long time bins over the course of the experiment reached significance ($ts_{27} < 1.801$, $ps > 0.083$, $ds_z < 0.340$). Fourth, relative to sham, the frontal-alone and temporal-alone theta-tuned montages had no significant impact on performance during the post-stimulation period or at any individual time bin during or after stimulation ($ts_{27} < 1.049$, $ps > 0.303$, $ds_z < 0.198$) (similar results were obtained using 1.6 mA HD-tACS, see Methods).

The results from Experiment 2 suggest that the spectral nature of individual brain network synchronization may be an important consideration when designing personalized interventions aimed at increasing working memory function. The results from Experiment 2 also suggest that a concurrent modulation of prefrontal and temporal regions may be necessary to effectively manipulate the frontotemporal circuit and boost cognitive performance. Future neuroimaging studies combined with HD-tACS will be helpful in clarifying the precise brains areas responsible for these stimulation effects, including whether subcortical regions with nonzero time lag (perhaps remotely activated by stimulation) interact with prefrontal and temporal areas to facilitate changes in memory performance.

Changing HD-tACS phase angle provides bidirectional control of working memory performance in younger adults

Experiment 3 further examined the relationship between working memory and the timing of frontotemporal network dynamics (see Methods for details). In brief, we found that antiphase HD-tACS, designed to desynchronize cortical interactions between frontotemporal areas, rapidly induced working memory deficits in younger adults (Supplementary Fig. 2). The results across Experiments 1–3 suggest that by changing the phase angle of stimulation (inphase versus antiphase) we can change the direction of the causal effects on performance (improvement versus impairment). Finally, in Experiment 4, we sought to extend the stimulation benefits induced in older adults in Experiment 1 to poor performing younger subjects (see Methods for details and Supplementary Fig. 3). The results from Experiment 4 suggest that the HD-tACS improvement may be applicable to a wide range of individuals who exhibit suboptimal working memory function and reductions in synchronous neural activity.

Discussion

Here we show that a core feature of cognitive decline may emerge from the temporal decoupling of neural codes theorized to constitute a flexible frontotemporal circuit for the monitoring and storage of memory contents of real-world information. The work supports theories of neurocognitive aging that propose cortical disconnection underlies age-related cognitive decline [4–6, 9, 10], and suggests that aspects of neurocognitive aging may be related to the declining use of ubiquitous physiological mechanisms of cortical information gating and transmission, indexed by cross-frequency PAC and phase synchronization. However, the weakening of these mechanisms or the absence of their functioning does not appear to be immutable. We developed a noninvasive procedure for directly acting on these mechanisms by matching their preferred resonance frequency on an individual subject basis with that of

external alternating current. The results suggest that by customizing electrical stimulation to individual network dynamics it may be possible to influence putative signatures of intra- and inter-regional functional connectivity, and rapidly boost working memory performance accuracy in older adults, with effects that last for 50 minutes and potentially longer.

The memory-related PAC that was exogenously induced in older adults was estimated to arise from ventral stream regions nearest the temporal cortex (Fig. 3a). Despite the limitations of source reconstruction, the detection of neural generators in the temporal location is consistent with evidence from magnetoencephalography (MEG) [18, 30], neuroimaging [31, 32], human intracranial EEG [33, 34], and nonhuman primate single-unit recordings [35, 36], implicating areas of the ventral visual pathway in the working memory processing of natural objects. For example, using human intracranial EEG, areas of the temporal cortex and medial temporal lobe have been shown to interact via phase synchronization to support working memory maintenance [34], and it is possible that the theta-gamma PAC measured in the present study captured cortical interactions in this general region. Moreover, the PAC effect was left lateralized in electrode and source space. Previous studies using synchronization measures recorded by MEG [18, 30] and intracranial EEG [34] have found similar results, suggesting PAC and phase synchronization may be more prominent in the left hemisphere of temporal areas during working memory tasks with complex objects. However, why such behaviorally significant lateralized effects exist remains a topic of open investigation [37, 38]. Research employing neuromodulation techniques may be uniquely suited to help us better understand the contributions from each hemisphere. For example, it would be interesting to test whether theta-tuned HD-tACS can exert similar connectivity and behavioral benefits when targeting right lateralized regions, or whether only modulation of left frontotemporal cortex elicits working memory advantages.

The action mechanisms of tACS are generally thought to be entrainment of endogenous rhythms at the frequency of stimulation [39, 40] and induction of synaptic changes via spike-timing dependent plasticity [41, 42], the latter of which may underlie offline tACS effects on cortical rhythms and behavior [41]. Similarly, theories of PAC and phase synchronization propose that these coding schemes play a critical role in the support and promotion of synaptic plasticity, with some of the best-studied examples including theta-gamma PAC and theta phase synchronization within and between structures of the hippocampus and neocortex (e.g., prefrontal and temporal regions) during working memory, information encoding, and long-term memory retrieval [14]. Given previous research suggesting a general function of PAC and phase synchronization in synaptic plasticity [14, 43], prior work showing that phase synchronization can change spike time-dependent plasticity [44, 45], and the present results demonstrating offline stimulation effects for longer than 50 minutes, we speculate that the external manipulation of theta-gamma PAC and theta phase synchronization that improved behavior may be due to neuroplastic changes in functional connectivity. That is, by noninvasively intervening in the temporal synchronization patterns of large-scale human brain activity, the results suggest it may be possible to enhance the postsynaptic effect of spikes from one area on another, thereby improving neural communication associated with the control and storage of information in working memory. However, while the present work hints at this conclusion, further research is required to more thoroughly explore the

hypothesis that theta-tuned frontotemporal HD-tACS is capable of eliciting neuroplastic modifications in functional connectivity with direct and lasting behavioral consequences.

The improvement in working memory accuracy for older adults was observed to outlast the stimulation period and continue to the last measurable post-stimulation time point in Experiments 1 and 2, raising the possibility that subjects experienced improvements in working memory function that lasted longer than what could be evaluated in the present study. Future research will be important to determine the full time course of the stimulation-induced behavioral advantages and whether they can transfer to other working memory functions (e.g., capacity, updating, switching) and higher-order cognitive abilities that rely on working memory, such as language comprehension, mathematical competence, and decision-making. Research efforts in this direction should help set the groundwork necessary for developing future non-pharmacological interventions aimed at reducing cognitive deficits in physiological aging and clinical populations.

Methods

Subjects

No statistical methods were used to pre-determine sample sizes but our sample sizes are similar to those reported in previous publications [22, 23, 46]. 154 subjects gave written consent to procedures approved by the Boston University Institutional Review Board and were paid. Of the 91 subjects in Experiment 1, five were excluded due to excessive eye movements and two voluntarily withdrew before completing the study. Data on the remaining 84 subjects were analyzed. 42 subjects were younger adults aged 20 to 29 years old (mean age 24.4 ± 2.8 SD, 20 female, all right-handed, mean years of education 15.7 ± 1.3 SD), and 42 were older adults aged 60 to 76 years old (mean age 68.8 ± 4.4 SD, 22 female, all right-handed, mean years of education 17.0 ± 2.3 SD). Of the 31 subjects in Experiment 2, three voluntarily withdrew before completing the study. Data on the remaining 28 subjects (aged 62–75 years, mean age 69.6 ± 3.7 SD, 14 female, all right-handed, mean years of education 16.4 ± 1.4 SD) were analyzed. Of the 18 subjects in Experiment 3, data from all 18 subjects were analyzed (aged 21–28 years, mean age 25.3 ± 2.3 SD, 9 female, all right-handed, mean years of education 16.1 ± 1.2 SD). Of the 42 younger adults from Experiment 1, 14 of the poorest performers were re-recruited and successfully completed Experiment 4 (aged 21–29 years, mean age 26.8 ± 1.8 SD, 9 female, all right-handed, mean years of education 14.8 ± 1.1 SD).

All subjects reported no metal implants in head, no implanted electronic devices, no history of neurological problems or head injury, no skin sensitivity, no claustrophobia, not being pregnant, no current use of psychoactive medication, normal color vision, and normal or corrected-to-normal visual acuity. The Mini Mental State Examination (MMSE) [47] was used to screen older subjects for dementia. All subjects scored in the normal range (24–30). Mean (± SD) MMSE scores were 28.9 ± 1.1 for older adults and 29.5 ± 0.9 for younger adults in Experiment 1, 29.0 ± 0.9 for older adults in Experiment 2, 29.6 ± 0.7 for younger adults in Experiment 3, and 29.3 ± 1.2 for younger adults in Experiment 4. The Beck Depression Inventory (BDI-II) [48] was used to screen subjects for depression. No subjects met BDI-II criteria for depression (>13). Mean (± SD) BDI-II scores were 6.0 ± 5.2 for older adults and

6.1 ± 5.1 for younger adults from Experiment 1, 6.0 ± 4.8 for older adults from Experiment 2, 5.8 ± 4.9 for younger adults from Experiment 3, and 6.1 ± 5.3 for younger adults from Experiment 4. Of note, the smoking status of subjects was not obtained in the present experiments. However, given emerging evidence suggesting that smoking may increase risk of cognitive decline in the elderly and non-elderly [49], and that nicotine deprivation may reduce cognitive functions and task-related neurophysiology [50, 51], it will be important for future studies to investigate the possibility of smoking status interactions with the effects of noninvasive neuromodulation and measures of neural synchronization used in the present study.

Stimuli and Procedures

Overview.—In Experiment 1, younger adults visited the laboratory on two test days (one pre-experiment screening day and one experimental day). The experimental day consisted of recording EEG and behavior during and after the administration of sham HD-tACS. In Experiment 1, older adults visited the laboratory on three separate test days (one pre-experiment screening day and two experimental days). On the experimental days, subjects had their EEG and behavior recorded during and after the administration of frontotemporal inphase theta-tuned and sham HD-tACS (Fig. 1a). The two-day design for older adults was double blind, sham-controlled, and within-subjects, with stimulation order counterbalanced across subjects. HD-tACS was administered over the first 10 blocks (or ~25 minutes) of the task (Fig. 1b). After stimulation, all subjects continued to perform the task for another 20 blocks (or ~50 minutes). Behavioral data were analyzed during and after stimulation, whereas EEG data were analyzed on post-stimulation blocks only to avoid potential confounds associated with tACS [52, 53]. Experiment 2 was similar to Experiment 1, but only behavior was collected, and the experiment consisted of six days in which a new group of older adults participated in one pre-experiment screening day and five experimental days. The design was double blind, sham-controlled, within-subjects, with stimulation order randomized across subjects. Each subject received: (i) sham stimulation to replicate the age-related working memory deficits observed at baseline in Experiment 1, (ii) frontotemporal inphase theta-tuned stimulation (Fig. 1a) to replicate the working memory benefit of stimulation relative to sham in Experiment 1, (iii) unifocal frontal theta-tuned stimulation (Fig. 5a) and (iv) unifocal temporal theta-tuned stimulation (Fig. 5b) on separate days to test the anatomical specificity of the multifocal frontotemporal montage, and (v) frontotemporal inphase 8-Hz nontuned stimulation (Fig. 1a) to test the frequency specificity and need for personalized intervention. Experiment 3 consisted of one screening day and two experimental test days involving sham and frontotemporal antiphase theta-tuned HD-tACS (counterbalanced across subjects), in which the behavior of younger adults was recorded "online" (i.e., during the 10-block delivery period of sham or active stimulation). Experiment 4 involved re-recruiting poor performing younger adults from Experiment 1 and running them through the frontotemporal inphase theta-tuned HD-tACS condition using a 10-block pre-stimulation baseline, 10-block stimulation period, and 10-block post-stimulation period.

Experimental task.—In the experiments, subjects performed a change-detection task using images of natural objects (Fig. 1b) drawn from 6,800 unique real-world, high-quality

objects from Konkle et al. (2010) [54] and Brady et al. (2010) [55]. We designed the task to have two different conditions: a memory block and a non-memory vigilance control block. The memory and control blocks were matched on perceptual and attentional demands, which allowed us to better isolate the neural processes related to memory maintenance within each age group, while reducing effects of memory-unspecific and stimulus-driven processes [18, 56].

In the memory block, each trial began with a central fixation cross (<0.01 cd/m^2, 0.4 × 0.4° of visual angle, 800–1200 ms, randomly jittered with a rectangular distribution), followed by a high-quality picture of an object with texture and color (200 ms). After a delay period (3000 ms) during which no information was presented, a probe stimulus appeared (200 ms), which was either identical to the previously presented target or a slightly modified version of the target (50% of all trials, randomly interleaved). The modifications of target stimuli consisted of changes based on adding, removing, distorting, or rotating individual object features. Subjects were instructed to store the target in memory over the delay period and report whether or not the probe stimulus was the same or different from the target by pressing a gamepad button as quickly and accurately as possible using the thumb of their right hand. Subjects received performance accuracy feedback at the end of every trial (200 ms).

In the non-memory vigilance control block, the trial sequence was identical to the memory block with the exception of the probe stimulus. On control trials, in place of a probe stimulus, after the delay period, a grating stimulus (30 ms) was presented followed by a backward mask (a plaid, tilted at 45°, 120 ms). The grating stimulus was a vertically oriented square-wave grating with a maximum 3 cycles per degree of contrast, subtending 4° of visual angle. Subjects were instructed not to remember the target stimulus but instead to determine whether the grating was tilted clockwise (50% of trials, randomly interleaved) or counterclockwise from the vertical. Performance difficulty was dynamically adjusted on a trial-by-trial basis using five possible magnitudes of orientation changing logarithmically from 0.3° to 5° to the vertical. Trial-by-trial adjustments on control trials were based on subjects' performance on memory trials.

All trials contained unique stimulus pairs of a target and probe. The memory and control blocks were administered blockwise in alternating order. Subjects were informed about the upcoming block prior to the start of each block. Each experimental test day (i.e., each stimulation condition) consisted of 30 total blocks (15 blocks of memory trials, 15 blocks of control trials, with 26 trials per block), with the exception of Experiment 3, which consisted of 10 total blocks. Task duration for each experiment was approximately 75 minutes, except Experiment 3, which lasted approximately 25 minutes.

Electroencephalography.—EEG and behavior were recorded in a dimly lit, electrically shielded, sound attenuated chamber to avoid line noise interference and reduce the possibility of subject-experimenter interaction during testing. HD-tACS Ag/AgCl electrodes and actiCap slim active EEG electrodes were mounted in a BrainCap elastic cap for 128 electrodes prepared with super-visc high-viscosity electrolyte gel (Brain Products GmbH, Germany). EEG was collected from 96 electrodes arrayed according to the international 10–20 system using an ActiChamp active channel amplifier sampling at 1000 Hz. The right

mastoid electrode served as the online reference. Horizontal eye position was monitored by recording the electrooculogram from bipolar electrodes placed at the outer canthi of each eye, and vertical eye position and blinks were monitored with bipolar electrodes placed above and below the left orbit. All EEG processing and analysis were conducted using Matlab scripts calling on the Fieldtrip toolbox [57].

High-definition transcranial alternating-current stimulation.—The alternating-current stimulation was administered noninvasively using an M x N 9-channel high-definition transcranial electrical current stimulator (Soterix Medical, New York, NY). The HD-tACS procedures included multiple sintered 12-mm diameter Ag/AgCl electrodes, attached to custom high-definition plastic holders, filled with conductive gel, and embedded in the BrainCap. Electrode placement was guided by current-flow modeling using HD-Explore and HD-Targets (Soterix Medical, New York, NY), with the goal of targeting the left prefrontal cortex and the left temporal cortex. The selection of these regions was based on a pilot study of ten subjects, in which data-driven coupling analyses (described below) identified the involvement of these regions during the memory versus non-mnemonic blocks of the change-detection task. Figure 1a shows the stimulation parameters (i.e., electrode number, electrode location, and current intensity values) of the multifocal frontotemporal inphase montages. Figure 5a shows the stimulation parameters of the unifocal frontal montage targeting left prefrontal cortex. Figure 5b shows the stimulation parameters of the unifocal temporal montage targeting the left temporal cortex. A bipolar sinusoidal alternating current was applied at either an individual subject defined theta-band frequency (i.e., the theta-tuned condition) or at 8-Hz for all subjects (i.e., the 8-Hz nontuned condition). Stimulation intensity (peak to peak) was set to 1.6 mA for the frontotemporal montages, 1.0 mA for the temporal montage, and 0.6 mA for the frontal montage.

The choice of stimulation intensities for the temporal-alone and frontal-alone montages (Fig. 5a, b) was guided by current-flow modeling, which estimated that these stimulation intensities would reach their respective cortical targets with electric field strength similar as those produced by the frontotemporal montage (Fig. 1a). However, it is possible that the stimulation intensities used in Experiment 2 were not strong enough to effectively modulate these regions, individually, and that higher intensities (e.g., > 1.0 mA) are required to induce significant behavioral changes. To address this question, we invited back all subjects from Experiment 2 to participate in an additional two test days, in which the frontal-alone and temporal-alone montages were applied with the same stimulation intensity as the frontotemporal montage (i.e., 1.6 mA). Consistent with results from Experiment 2 (Fig. 6), we observed no significant RT or accuracy differences between sham and the frontal-alone or temporal-alone theta-tuned montages ($ts_{27} < 0.813$, $ps > 0.423$, $ds_z < 0.154$).

For all montages, stimulation was applied for 10 blocks of trials (i.e., 5 memory blocks and 5 control blocks, alternating in order, lasting approximately 25 minutes). In the frontotemporal montages (i.e., theta-tuned and 8-Hz nontuned) across Experiments 1, 2, and 4, the alternating current was inphase, meaning it was delivered with 0° relative phase difference across the two targeted cortical locations. We specifically used inphase stimulation because it has been shown to facilitate network synchronization between targeted regions and improve cognitive performance [21–23, 46, 58]. In contrast, for Experiment

3, subjects were challenged with a frontotemporal theta-tuned antiphase montage, in which alternating current was delivered with 180° relative phase difference across targeted areas, with the goal of impeding network synchronization and impairing performance [21]. The current intensity values for the antiphase montage were set to: E12 = 0.267, E27 = 0.267, E29 = 0.267, G32 = −0.267, L4 = −0.267, K5 = −0.267. Although induction of peripheral flicker perception is typically only reported when using higher frequency tACS [59–61], we nonetheless used post-experiment questionnaires to confirm that our low-frequency stimulation procedure did not induce peripheral flicker perception. All subjects confirmed that stimulation was acceptable and did not induce painful skin sensations or phosphenes.

Dynamic systems theory predicts that systems with intrinsic periodic dynamics have preferred stimulation frequencies (or "resonance frequencies") and that neuronal modulation should be strongest or most effective when the exogenous stimulation frequency of weak periodic perturbations is at or near the brain network's resonance frequency [39]. To design personalized interventions, we determined each subject's endogenous theta peak frequency of their memory-related frontotemporal network by administering a brief (~25 minutes) pre-experiment EEG recording while subjects performed an abbreviated version of the change-detection task (i.e., 10 blocks). All subjects completed the pre-experiment EEG session on their screening day, which preceded all experimental test days. Single-trial spectral decomposition was performed from 1–30 Hz in 0.1-Hz increments on −2000 to 5000 ms segments peri-target onset, and was accomplished using complex Morlet wavelets with the constant ratio of the center frequency set to 14 and the number of cycles included in the mother wavelet set to 6 to increase frequency resolution. Long-range theta-band synchronization was assessed from 4–8 Hz in 0.1-Hz increments and computed using PLV [62] in source space between left temporal cortex and left prefrontal cortex during memory maintenance (500 to 3000 ms post-target onset) on memory versus control blocks. Within the theta band, the frequency with maximum mean PLV was extracted on an individual subject basis and served as the target stimulation frequency. Individually frequency-tuned stimulation was applied with 0.5-Hz resolution, rounding up from 0.3 Hz. For example, an individual with a peak synchronization frequency of 7.2 Hz was given 7-Hz stimulation, whereas an individual with a peak at 7.3 Hz was given 7.5-Hz stimulation.

We took several measures to ensure that information about the experiments would not lead to biasing of results, using previously established methods [21, 58, 63–68]. First, all experiments were within-subjects in design, meaning each older adult (in Experiments 1 and 2) or younger adult (in Experiments 3 and 4) performed all levels of the independent variable (i.e., every stimulation condition) to eliminate confounds related to subject differences. Second, the experiments were sham-controlled. The sham stimulation condition followed the same procedure as the active theta-tuned frontotemporal condition, but stimulation only lasted 30 seconds, ramping up and down at the beginning and end of the 10-block period, simulating the tingling sensation that subjects typically experience and then quickly habituate to during active stimulation [67]. Of note, while the sham condition implemented here is considered a gold standard in brain stimulation research, the present study benefited from several additional stimulation controls, such as the pre-stimulation baseline of Experiment 4 and the frontotemporal nontuned condition of Experiment 2. The latter condition stands as a particularly robust control because unlike the sham condition the electrical current of the

nontuned montage was running throughout the entire 10-block duration and at 1.6 mA intensity. Third, we used a double blind method in which a second experimenter set the mode (e.g., active or sham) on the stimulator, but otherwise did not interact with the subject or the experimenter who performed data collection. Fourth, we conducted recordings in a sound-attenuated, electrically shielded chamber to eliminate subject-experimenter interaction, which could have at least implicitly biased the subjects. Fifth, the test days for each subject were separated by at least one week to avoid potential carryover effects from the stimulation. Sixth, we confirmed that subjects were blind to the presence of the stimulation. After each test day, we administered a safety questionnaire [69] and visual analog scale [70], which included questions regarding attention, concentration, mood, vision, headache, fatigue, and skin sensations under the stimulating electrodes. Scores on these ratings did not significantly differ by stimulation condition (Experiment 1, $Fs_{1, 41} < 0.322$, $ps > 0.574$; Experiment 2, $Fs_{4, 108} < 0.446$, $ps > 0.669$; Experiment 3, $Fs_{1, 17} < 0.693$, $ps > 0.417$; Experiment 4, $Fs_{1, 13} < 1.168$, $ps > 0.299$). In addition, all subjects were asked at the end of the experiment whether they could guess the presence of stimulation and were at chance levels (Experiment 1, 52.4% hit rate; Experiment 2, 19.0% hit rate; Experiment 3, 55.6% hit rate; Experiment 4, 55.0% hit rate). Finally, to avoid expectancy and demand characteristic effects, in Experiment 1 all younger adults were treated the same as the older adults in the sham condition, that is, HD-tACS electrodes were placed, and the sham stimulation was used to induce the same itching and tingling experienced by older adults.

Data Analysis

Behavioral preprocessing.—We calculated mean and standard deviations of accuracy and RTs for each memory and control block, and each subject and stimulation condition from data recorded before, during, and after the administration of HD-tACS, depending on the experiment. RTs deviating 2.5 standard deviations from the mean of each subject were defined as outliers and discarded. RT and accuracy results from the non-memory control block did not significantly differ from those of the memory block for either age group or stimulation condition (Experiment 1, RT $ts_{41} < 0.683$, $ps > 0.498$; accuracy, $ts_{41} < 0.626$, $ps > 0.535$; Experiment 2, RT $ts_{27} < 0.321$, $ps > 0.750$; accuracy $ts_{27} < 0.641$, $ps > 0.527$; Experiment 3, RT $ts_{17} < 0.604$, $ps > 0.554$; accuracy, $ts_{17} < 1.141$, $ps > 0.270$; Experiment 4, RT $ts_{13} < 0.857$, $ps > 0.407$; accuracy, $ts_{13} < 1.392$, $ps > 0.187$), confirming the success of the trial-by-trial dynamic adjustment procedure we used for matching difficulty level across blocks.

Electroencephalographic preprocessing.—Offline, EEG data recorded immediately after HD-tACS administration were re-referenced to the average of the left and right mastoids, high-pass filtered at 0.1 Hz, and low-pass filtered at 170 Hz. Segments were cut −2000 to 5000 ms with respect to target onset. Using large segments allowed us to avoid edge artifacts caused by wavelet convolution during the memory maintenance period (i.e., 500 to 3000 ms post-target onset). Of note, although the comparison of data between memory and control blocks (described below under *Statistics*) allowed us to better isolate working memory related neural activity and reduce the influence of evoked activity and stimulus-driven processes, we nonetheless confirmed the statistical significance of all primary EEG results using the more conservative analytic window of 1000 to 3000 ms post-

target onset. Visual inspection was initially used to remove large muscle artifacts, followed by an independent component analysis [71] to remove blink and noise artifacts [72]. This resulted in an average 13.8 ± 5.8 components rejected.

Time-frequency analysis.—The EEG time series in each trial was convolved with a set of complex Morlet wavelets, defined with a Gaussian envelop using a constant ratio $\left(\sigma_f = \frac{f}{7}\right)$ and a wavelet duration $\left(6\sigma_t\right)$, where f is the center frequency and $\sigma_t = \frac{1}{2\pi\sigma_f}$. Frequencies ranged from 1 to 120 Hz in 1-Hz increments.

Electrode-level phase-amplitude coupling.—We computed within-electrode PAC during the delay period between memory and control blocks using combinations of phase frequencies and amplitude frequencies, and then cluster based permutations statistics were used to identify memory-specific spatiospectral clusters for each age group and stimulation condition.

To assess PAC, we calculated circular-linear correlations [73]. This method allowed us to examine the relationship between circular phase and linear amplitude variables across trials by linearizing the phase variable into *sin* and *cos* components and computing a single correlation coefficient according to the following formula:

$$\rho\phi a = \sqrt{\frac{r_{ca}^2 + r_{sa}^2 - 2r_{ca}r_{sa}r_{cs}}{1 - r_{cs}^2}}$$

$$r_{ca} = c(cos\phi[n], a[n])$$

$$r_{sa} = c(sin\phi[n], a[n])$$

$$r_{cs} = c(sin\phi[n], cos\phi[n])$$

$c(x, y)$ = Pearson correlation between x and y

$\phi[n]$ = instantaneous phase

$a[n]$ = instantaneous analytic amplitude

To examine the extent to which specific low-frequency phase and high-frequency amplitude values were coupled, we calculated circular-linear correlations using phase frequencies between 2 and 16 Hz in 2-Hz increments and amplitude frequencies between 18 and 120 Hz in 4-Hz increments, collapsed across trials and time within each trial, for each subject, block, stimulation condition, and electrode. The correlation coefficients were normalized

using the standard Fisher r-to-z transformation. Of note, similar PAC results were obtained using a narrower range of amplitude frequencies from 18 to 58 in 4-Hz increments.

To examine the phase-angle preference of the theta-gamma PAC effect, we examined phase-sorted amplitude values based on the phase frequency, amplitude frequency, and electrodes showing significant memory-related PAC. The theta phase and gamma amplitude values were aligned and sorted into two vectors by phase angles in ascending order for each subject, collapsed across time and trials. Amplitude values were sorted based on the corresponding phase angle. Phase angles were grouped into 30 bins of 12-degree increments and the amplitudes were averaged within each phase bin (Fig. 3c shows plots of 6 bins of 60 degrees each for visualization purposes). Of note, although the phase bin number is arbitrary, the specific number does not influence PAC estimation [74]. We normalized the individual amplitude distribution by the mean across all bins.

Source-level phase-amplitude coupling.—To estimate potential neural generators, we projected data of each trial into source space using the linearly constrained minimum variance (LCMV) beamformer, which estimates brain activity separately for each source location by minimizing the variance of the filtered signal with the unit-gain constraint [75]. The LCMV is widely used for source reconstruction [76] because it provides higher spatial resolution compared to linear inverse methods [77, 78]. Source estimation was facilitated by generating a realistically shaped, sufficiently detailed, volume conduction head model comprised of different tissues classes for white (0.14 S/m) and gray (0.33 S/m) matter, compact (0.0064 S/m) and spongy (0.02864 S/m) bone, and cerebral spinal fluid (1.79 S/m) and skin (0.43 S/m) [79, 80] using CURRY 7.0 multimodal neuroimaging software (Compumedics Neuroscan, Charlotte, NC). This 5-layer approach was recently shown to reduce considerable inverse, connectivity, and topographical errors when computing connectivity in source space, as compared with conventional 3-layer models of skin, skull, and brain [81]. A finite element method, which allows for modeling arbitrary anisotropic conductivity profiles, was used to solve the EEG forward problem [82–84]. Leadfields were calculated for sources on a regularly spaced grid with 1 cm distance covering the entire brain (3294 voxels) in Montreal Neurological Institute (MNI) space. Subject-specific 3D electrode positions were obtained with the CapTrak electrode localization tool (Brain Products GmbH, Germany) and results were aligned to the MNI template brain. Anatomical labeling of voxels was performed with NFRI functions [85] based on the automated anatomical labeling atlas [86] and automated Talairach atlas labels [87]. PAC in source space was calculated in the same fashion as PAC in electrode space using circular-linear correlations. It is important to note that although source reconstruction methods allow us to sharpen our reasoning about the underlying pattern of activity generating the scalp-recorded EEG signal, such modeling carries with it several ambiguities. As a result, source estimates are not intended as strong claims about the precise spatial origins of neuronal generation, but rather as potential candidate regions with which to further investigate using methods with higher spatial resolution, such as fMRI and intracranial neurophysiological recordings.

Cross-frequency phase-slope index.—To determine whether low-frequency phase was driving high-frequency amplitude during memory maintenance or vice versa, we

calculated the cross-frequency PSI [88]. To avoid edge artifacts, we used relatively long segments of 2500 ms (500 to 3000 ms post-target onset), which included at least 5 cycles of the slowest rhythm (6.5 Hz), consistent with previous reports [88]. We considered frequencies between 6.5 and 10.5 Hz (0.5-Hz increments) after applying a Hanning window and extracting the complex Fourier coefficients. Significant values above zero indicate that low-frequency components are driving high-frequency activity, while negative values indicate the opposite direction of influence, and values nearest zero suggest no directional coupling.

Seeded source-level phase-locking value.—To evaluate long-range cortical interactions between regions exhibiting local PAC and more distant brain areas, we computed PLV [62] between pairs of voxels for the low- and high-frequency bands involved in PAC.

PLV was computed using the following formula:

$$PLV = 1/N\left|\sum_{n=1}^{N} e^{i\left(\theta_1(n) - \theta_2(n)\right)}\right|$$

where N is the number of sampled time points and θ_1 and θ_2 are the instantaneous phase values at time point n.

The seed region and frequencies chosen for the PLV analysis were based on the location and frequencies involved in significant changes in PAC. Because no localized sources of PAC were observed for older adults in the sham condition of Experiment 1, we used the seed region identified from younger adults in the sham condition. However, we confirmed the results from this analysis by recalculating source PLV for older adults in the sham condition using seed regions defined by significant PAC identified from the active stimulation condition in the same subjects. For the seeded PLV analysis, we averaged the cross-spectral density matrices between 500 and 3000 ms in each condition and projected the results of each frequency bin within the theta or gamma band in source space using the dynamic imaging of coherent sources beamformer (see PAC section for description of forward model) [89]. For each frequency bin separately, PLV was computed from every seed voxel to all other voxels in the 3294 grid, averaged across all considered frequency bins, and Fisher z transformed. This resulted in two synchronization measures per voxel, one for the memory and one for the control block, for each age group and stimulation condition.

Within-frequency phase-slope index.—To determine the directionality of the long-range connections in source space, we computed PSI [90], an estimate of the direction of information flow between two signals. PSI was computed between voxels that showed a significant difference in PLV between memory and control blocks. For each considered voxel pair, the PLV was calculated at each frequency bin within the frequency band of interest for both blocks, separately. Then, the PSI was computed for each block, stimulation condition, and age group across all frequency bins within this frequency band as described by Nolte et al. (2008) [90]. A positive PSI indicates that the seed region acts as a sender, and negative values provide evidence for the seed region acting as a receiver.

Alpha power analysis.—We used posterior alpha power, a putative marker of the strength of visual attention [91, 92], to evaluate the effects of age and exogenous stimulation on visual attention of the target stimuli presented in the task. Following single-trial spectral decomposition, we extracted, squared, and averaged the magnitude length of the complex number vectors, yielding a measure of intertrial total spectral power for a given frequency, time point, and electrode. Power values were baseline corrected (−200 to 0 ms prior to target onset) by calculating the relative signal change where $P_{corrected}(t,f) = P(t,f) - P_{baseline}(f)/P_{baseline}(f)$ for the individual frequencies. Analysis focused on alpha-band frequencies (8–14 Hz) during a conservatively broad temporal window (100 to 400 ms after target onset), collapsed across occipital and parietooccipital electrodes on memory blocks.

Statistics

The neural and behavioral data met the assumptions of the statistical tests used. Data normality was confirmed with the Shapiro-Wilk test ($p > 0.05$). We used independent samples two-tailed *t*-tests to examine differences in mean RT on correct trials and accuracy between the different groups of subjects. We used paired sample two-tailed *t*-tests to examine differences in mean RT on correct trials and accuracy within the same group of subjects between stimulation conditions. To assess within-session behavioral dynamics, we sorted the data from memory blocks into nine sequential 4-minute-long bins (with approximately 4 minutes between each bin from control blocks). To examine changes in behavior at each time bin we used two-tailed *t*-test. To examine behavioral changes across time bins we used repeated measures analyses of variance (ANOVAs) with the within-subjects factor of time bin (1 vs. 2 vs. 3 vs. 4 vs. 5 vs. 6 vs. 7 vs. 8 vs. 9) and the between-subjects factor of stimulation condition (sham vs. active) or age group (young vs. old).

We used cluster-based permutation tests [93] implemented in FieldTrip, which corrects for multiple comparisons. PAC analysis was computed between memory and control blocks for the amplitude frequencies of interest, the phase frequencies of interest, and all electrodes. A *t*-test was calculated at every electrode separately. Neighboring electrodes in terms of space, phase frequency, and amplitude frequency that fell below a *p*-value of 0.05 were grouped into clusters. Within each cluster, the sum of *t*-values was then calculated. A null distribution was generated using permutated data across subjects (1000 permutations). We calculated the maximum cluster-level test statistic, which provided a corrected *p*-value for each cluster. Clusters with a $p_{\text{corrected}} < 0.01$ (two-sided) were considered significant.

To examine block (memory, control) x age group (young, old), and block (memory, control) x stimulation (sham, active) interactions on memory-specific PAC, we performed linear regression using regressors representing these interactions, allowing us to assess PAC across the full frequency spectrum of the analysis. We used cluster permutation statistics corrected for multiple comparisons to test for significance. Neighboring phase and amplitude frequencies that fell below a *p*-value of 0.05 were grouped into clusters. A null distribution was created with permutated data across subjects (1000 permutations). To do this, we performed an identical analysis to that described above, except instead of using the actual regressor of block and age group, or block and stimulation condition, we randomly shuffled

the values in those regressors. For example, we randomly assigned data to memory block versus control block and sham versus active conditions. We calculated the maximum cluster-level test statistic, providing a corrected p-value for each cluster. Clusters with a $p_{corrected} < 0.01$ were considered significant.

For the phase-sorted amplitude analysis, to test if the gamma-amplitude values (26–34 Hz) systematically changed across the cycle of theta-phase angles (8 Hz), we used a nonparametric Wald-Wolfowitz run test of randomness to determine whether the phase-ordered amplitude bins significantly deviated from a uniform distribution. A significant result indicates that the phase-binned amplitude values exhibit a systematic order.

For seeded source-level PLV analysis, PLVs were averaged across all considered seed voxels within each condition. We statistically compared the memory against control blocks by computing two-tailed, paired sample t-tests in each voxel and used cluster permutations statistics with the spatial cluster dimension to control for multiple comparisons (uncorrected cluster $\alpha = 0.01$). Of note, we obtained similar results when employing another common neural connectivity measure called the imaginary part of coherency, which is a calculation confined to non-instantaneous correlations (i.e., correlations exclusively with non-zero phase lag), and thus insensitive to false connectivity arising from volume conduction [94].

For within-frequency PSI analysis, we averaged the PSI values across all voxel pairs within the cluster and used paired t-tests to evaluate differences in directionality between the memory and control blocks for each age group and stimulation condition.

To assess relationships between PAC and performance accuracy, we used bivariate linear regression analysis (Pearson correlation, two-tailed) between individual subject percentage correct accuracy scores and memory-specific theta-gamma PAC collapsed across left temporal electrodes.

Alpha power analysis focused on the mean spectral power from 8–14 Hz, 100–400 ms post-target onset, collapsed across occipital and parietooccipital electrodes on memory blocks. We used two-tailed t-tests to compare power values across age groups and stimulation conditions. We confirmed the results of this hypothesis-driven approach with a hypothesis-independent approach that makes no a priori assumptions about the precise spectral or temporal nature of the effect. For this analysis, power was averaged across occipital and parietooccipital electrodes, and assessed from 0 to 500 ms post-target onset in 10-ms increments for each frequency from 2 to 30 Hz in 1-Hz increments. Two-tailed t-tests were computed between age groups and stimulation conditions and a false discovery rate (FDR) was set to $\alpha = 0.01$ to control for multiple comparisons [95]. Results showed significantly ($p_{corrected} < 0.01$) greater alpha power reduction in younger relative to older adults in the sham condition from 130–360 ms and 9–11 Hz, and younger adults in the sham condition relative to older adults in the active condition from 140–300 ms and 10–12 Hz, but no modulations in older adults between sham and active conditions reached significance.

Effect sizes are reported as Cohen's d_z for t-tests and partial η^2 for ANOVAs.

Additional methods information can be found in the *Life Sciences Reporting Summary* associated with this paper.

Supplementary Material

Refer to Web version on PubMed Central for supplementary material.

Acknowledgements

This work was supported by a grant from the National Institutes of Health (R01 MH 114877) awarded to R.M.G.R.

References

1. Bishop NA, Lu T & Yankner BA Neural mechanisms of ageing and cognitive decline. Nature 464, 529–535 (2010). [PubMed: 20336135]
2. Hebert LE, Weuve J, Scherr PA & Evans DA Alzheimer disease in the United States (2010–2050) estimated using the 2010 Census. Neurology 80, 1778–1783 (2013). [PubMed: 23390181]
3. Hayutin AM Global demographic shifts create challenges and opportunities. PREA Quart, 46–53 (2007).
4. Park DC & Reuter-Lorenz PA The adaptive brain: aging and neurocognitive scaffolding. Nature Reviews Neuroscience 60, 173–196 (2009).
5. Grady C Trends in neurocognitive aging. Nature Reviews Neuroscience 13, 491–505 (2012). [PubMed: 22714020]
6. Hedden T & Gabrieli JD Insights into the ageing mind: a view from cognitive neuroscience. Nature Reviews Neuroscience 5, 87–96 (2004). [PubMed: 14735112]
7. Tomasi D & Volkow ND Aging and functional brain networks. Molecular Psychiatry 17, 549–558 (2012).
8. Andrews-Hanna JR, et al. Disruption of large-scale brain systems in advanced aging. Neuron 56, 924–935 (2007). [PubMed: 18054866]
9. Davis SW, et al. Assessing the effects of age on long white matter tracts using diffusion tensor tractography. NeuroImage 46, 530–541 (2009). [PubMed: 19385018]
10. O'Sullivan M, et al. Evidence for cortical "disconnection" as a mechanism of age-related cognitive decline. Neurology 57, 632–638 (2001). [PubMed: 11524471]
11. Siegel M, Donner TH & Engel AK Spectral fingerprints of large-scale neuronal interactions. Nature Reviews Neuroscience 13, 121–134 (2012). [PubMed: 22233726]
12. Roux F & Uhlhaas PJ Working memory and neural oscillations: alpha-gamma versus theta-gamma codes for distinct WM information? Trends in Cognitive Sciences 18, 16–25 (2014). [PubMed: 24268290]
13. Helfrich RF & Knight RT Oscillatory dynamics of prefrontal cognitive control. Trends in Cognitive Sciences 20, 916–930 (2016). [PubMed: 27743685]
14. Fell J & Axmacher N The role of phase synchronization in memory processes. Nature Reviews Neuroscience 12, 105–118 (2011). [PubMed: 21248789]
15. Sarnthein J, Petsche H, Rappelsberger P, Shaw G & von Stein A Synchronization between prefrontal and posterior association cortex during human working memory. Proceedings of the National Academy of Sciences of the USA 95, 7092–7096 (1998). [PubMed: 9618544]
16. Axmacher N, et al. Cross-frequency coupling supports multi-item working memory in the human hippocampus. Proceedings of the National Academy of Sciences 107, 3228–3233 (2010).
17. Fries P Rhythms for cognition: communication through coherence. Neuron 88, 220–235 (2015). [PubMed: 26447583]
18. Daume J, Gruber T, Engel AK & Friese U Phase-amplitude coupling and long-range phase synchronization reveal frontotemporal interactions during visual working memory. Journal of Neuroscience 37, 313–322 (2017). [PubMed: 28077711]

19. Sreenivasan KK, Curtis CE & D'Esposito M Revisiting the role of persistent neural activity during working memory. Trends in Cognitive Sciences 18, 82–89 (2014). [PubMed: 24439529]
20. Lara AH & Wallis JD Executive control processes underlying multiitem working memory. Nature Neuroscience 17, 876–883 (2014). [PubMed: 24747574]
21. Reinhart RMG Disruption and rescue of interareal theta phase coupling and adaptive behavior. Proceedings of the National Academy of Sciences, USA 114, 11542–11547 (2017).
22. Helfrich RF, et al. Selective modulation of interhemispheric functional connectivity by HD-tACS shapes perception. Public Library of Sciences Biology 12, e1002031 (2014).
23. Polanía R, Nitsche MA, Korman C, Batsikadze G & Paulus W The importance of timing in segregated theta phase-coupling for cognitive performance. Current Biology 14, 1314–1318 (2012).
24. Wolinski N, Cooper NR, Sauseng P & Romei V The speed of parietal theta frequency drives visuospatial working memory capacity. Public LIbrary of Sciences Biology 16, e2005348 (2018).
25. Alekseichuk I, Turi Z, Amador de Lara G, Antal A & Paulus W Spatial working memory in humans depends on theta and high gamma synchronization in the prefrontal cortex. Current Biology 26, 1513–1521 (2016). [PubMed: 27238283]
26. Salthouse TA The aging of working memory. Neuropsychology 8, 535–543 (1994).
27. Voytek B, et al. Age-related changes in 1/f neural electrophysiological noise. Journal of Neuroscience 35, 13257–13265 (2015). [PubMed: 26400953]
28. Cole SR & Voytek B Brain oscillations and the importance of waveform shape. Trends in Cognitive Sciences 21, 137–149 (2017). [PubMed: 28063662]
29. Scheffer-Teixeira R & Tort AB On cross-frequency phase-phase coupling between theta and gamma oscillations in the hippocampus. Elife 5, 423–435 (2016).
30. Daume J, Graetz S, Gruber T, Engel AK & Friese U Cognitive control during audiovisual working memory engages frontotemporal theta band interactions. Scientific Reports 7, 12585 (2018).
31. Ranganath C & D'Esposito M Medial temporal lobe activity associated with active maintenance of novel information. Neuron 31, 865–873 (2001). [PubMed: 11567623]
32. Nichols EA, Kao YC, Verfaellie M & Gabrieli JD Hippocampus, working memory and long-term memory for faces: evidence from fMRI and global amnesia for involvement of the medial temporal lobes. Hippocampus 16, 604–616 (2006). [PubMed: 16770797]
33. Axmacher N, et al. Sustained neural activity patterns during working memory in the human medial temporal lobe. Journal of Neuroscience 27, 7807–7816 (2007). [PubMed: 17634374]
34. Axmacher N, Schmitz DP, Wagner T, Elger CE & Fell J Interactions between medial temporal lobe, prefrontal cortex, and inferior temporal regions during visual working memory: a combined intracranial EEG and functional magnetic resonance imaging study. Journal of Neuroscience 28, 7304–7312 (2008). [PubMed: 18632934]
35. Lueschow A, Miller EK & Desimone R Inferior temporal mechanisms for invariant object recognition. Cerebral Cortex 5, 523–531 (1994).
36. Woloszyn L & Sheinberg DL Neural dynamics in inferior temporal cortex during a visual working memory task. Journal of Neuroscience 29, 5494–5507 (2009). [PubMed: 19403817]
37. Powell HW, et al. Material-specific lateralization of memory encoding in the medial temporal lobe: blocked versus event-related design. Neuroimage 27, 231–239 (2005). [PubMed: 15927485]
38. Henson R A mini-review of fMRI studies of human medial temporal lobe activity associated with recognition memory. Quarterly Journal of Experimental Psychology 58, 340–360 (2005). [PubMed: 16194973]
39. Ali MM, Sellers KK & Frohlich F Transcranial alternating current stimulation modulates large-scale cortical network activity by network resonance. Journal of Neuroscience 33, 11262–11275 (2013). [PubMed: 23825429]
40. Herrmann CS, Rach S, Neuling T & Strüber D Transcranial alternating current stimulation: a review of the underlying mechanisms and modulation of cognitive processes. Frontiers in Human Neuroscience 7 (2013).

41. Vossen A, Gross J & Thut G Alpha power increase after transcranial alternating current stimulation at alpha frequency (α-tACS) reflects plastic changes rather than entrainment. Brain Stimulation 8, 499–508 (2015). [PubMed: 25648377]
42. Zaehle T, Rach S & Herrmann CS Transcranial alternating current stimulation enhances individual alpha activity in human EEG. Public Library of Sciences ONE 5, e13766 (2010).
43. Bergmann TO & Born J Phase-amplitude coupling: A general mechanism for memory processing and synaptic plasticity? Neuron 97, 10–13 (2018). [PubMed: 29301097]
44. Gregoriou GG, Gotts SJ, Zhou H & Desimone R High-frequency, long-range coupling between prefrontal and visual cortex during attention. Science 324, 1207–1210 (2009). [PubMed: 19478185]
45. Wang XJ Neurophysiological and computational principles of cortical rhythms in cognition. Physiological Reviews 90, 1195–1268 (2010). [PubMed: 20664082]
46. Violante IR, et al. Externally induced frontoparietal synchronization modulates network dynamics and enhances working memory performance. Elife 6, e22001 (2017). [PubMed: 28288700]
47. Folstein M, Folstein SE & McHugh PR "Mini-mental state." A practical method for grading the cognitive state of patients for the clinician. Journal of Psychiatric Research 12, 189–198 (1975). [PubMed: 1202204]
48. Beck AT, Steer RA & Brown GK Manual for the beck depression inventory (The Psychological Association, San Antonio, TX, 1996).
49. Sabia S, et al. Impact of smoking on cognitive decline in early old age: the Whitehall II cohort study. Archives in General Psychiatry 69, 627–635 (2012).
50. Grundey J, Amu R, Batsikadze G, Paulus W & Nitsche MA Diverging effects of nicotine on motor learning performance: improvement in deprived smokers and attenuation in non-smokers. Addictive Behaviors 74, 90–97 (2017). [PubMed: 28600927]
51. Grundey J, et al. Double dissociation of working memory and attentional processes in smokers and non-smokers with and without nicotine. Psychopharmacology 232, 2491–2501 (2015). [PubMed: 25721074]
52. Noury N, Hipp JF & Siegel M Physiological processes non-linearly affect electrophysiological recordings during transcranial electric stimulation. Neuroimage 140, 99–109 (2016). [PubMed: 27039705]
53. Noury N & Siegel M Analyzing EEG and MEG signals recorded during tES, a reply. Neuroimage 167, 53–61 (2017). [PubMed: 29155079]
54. Konkle T, Brady TF, Alvarez GA & Oliva A Conceptual distinctiveness supports detailed visual long-term memory for real-world objects. Journal of Experimental Psychology: General 139, 558–578 (2010). [PubMed: 20677899]
55. Brady TF, Konkle T, Alvarez GA & Oliva A Visual long-term memory has a massive storage capacity for object details. Proceedings of the National Academy of Sciences 105, 14325–14329 (2008).
56. Park JY, Jhung K, Lee J & S.K., A. Theta-gamma coupling during a working memory task as compared to a simple vigilance task. Neuroscience Letters 532, 39–43 (2013). [PubMed: 23149131]
57. Oostenveld R, Fries P, Maris E & Schoffelen JM FieldTrip: Open source software for advanced analysis of MEG, EEG, and invasive electrophysiological data. Computational Intelligence and Neuroscience 2011, 1–9 (2011). [PubMed: 21837235]
58. Nguyen J, Deng Y & Reinhart RMG Brain-state determines learning improvements after transcranial alternating-current stimulation to fontal cortex. Brain Stimulation 11, 723–726 (2018). [PubMed: 29482970]
59. Kanai R, Chaieb L, Antal A, Walsh V & Paulus W Frequency-dependent electrical stimulation of the visual cortex. Current Biology 18, 1839–1843 (2008). [PubMed: 19026538]
60. Schutter DJ & Hortensius R Retinal origin of phosphenes to transcranial alternating current stimulation. Clinical Neurophysiology 121, 1080–1084 (2010). [PubMed: 20188625]
61. Paulus W On the difficulties of separating retinal from cortical origins of phosphenes when using transcranial alternating current stimulation (tACS). Clinical Neurophysiology 121, 987–991 (2010). [PubMed: 20181514]

62. Lachaux JP, Rodriguez E, Martinerie J & Varela FJ Measuring phase synchrony in brain signals. Human Brain Mapping 8, 194–208 (1999). [PubMed: 10619414]
63. Reinhart RMG, Zhu J, Park S & Woodman GF Medial-frontal stimulation enhances learning in schizophrenia by restoring prediction-error signaling. Journal of Neuroscience 35, 12232–12240 (2015). [PubMed: 26338333]
64. Reinhart RMG & Woodman GF Enhancing long-term memory with stimulation tunes visual attention in one trial. Proceedings of the National Academy of Sciences of the USA 112, 625–630 (2015). [PubMed: 25548192]
65. Reinhart RMG & Woodman GF Causal control of medial-frontal cortex governs electrophysiological and behavioral indices of performance monitoring and learning. Journal of Neuroscience 34, 4214–4227 (2014). [PubMed: 24647942]
66. Reinhart RMG, Zhu J, Park S & Woodman GF Synchronizing theta oscillations with direct-current stimulation strengthens adaptive control in the human brain. Proceedings of the National Academy of Sciences of the USA 112, 9448–9453 (2015). [PubMed: 26124116]
67. Reinhart RMG, Cosman JD, Fukuda K & Woodman GF Using transcranial direct-current stimulation (tDCS) to understand cognitive processing. Attention, Perception & Psychophysics 79, 3–23 (2017).
68. Reinhart RMG, Xiao W, McClenahan L & Woodman GF Electrical stimulation of visual cortex can immediately improve spatial vision. Current Biology 25, 1867–1872 (2016).
69. Poreisz C, Boros K, Antal A & Paulus W Safety aspects of transcranial direct current stimulation concerning healthy subjects and patients. Brain Research Bulletin 72, 208–214 (2007). [PubMed: 17452283]
70. Gandiga P, Hummel F & Cohen L Transcranial DC stimulation (tDCS): A tool for double-blind sham-controlled clinical studies in brain stimulation. Clinical Neurophysiology 117, 845–850 (2006). [PubMed: 16427357]
71. Jung TP, et al. Imaging brain dynamics using independent component analysis. The Proceedings of the Institution of Electrical and Electronic Engineers 89, 1107–1122 (2001).
72. Delorme A & Makeig S EEGLAB: An open source toolbox for analysis of singel-trial EEG dynamics including independent component analysis. Journal of Neuroscience Methods 134, 9–21 (2004). [PubMed: 15102499]
73. Berens P CircStat: a MATLAB toolbox for circular statistics. Journal of Statistical Software 31, 21 (2009).
74. van Driel J, Cox R & Cohen MX Phase-clustering bias in phase–amplitude cross-frequency coupling and its removal. Journal of Neuroscience Methods 254, 60–72 (2015). [PubMed: 26231622]
75. van Veen B, van Drongelen W, Yuchtman M & Suzuki A Localization of brain electrical activity via linearly constraint minimum variance spatial filtering. IEEE Translations on Biomedical Engineering 44, 867–880 (1997).
76. Hipp JF, Engel AK & Siegel M Oscillatory synchronization in large-scale cortical networks predicts perception. Neuron 69, 387–396 (2011). [PubMed: 21262474]
77. Sekihara K & Nagarajan SS Adaptive spatial filters for electromagnetic brain imaging (Springer, 2008).
78. Darvas F, Pantazis D, Kucukaltun-Yildirim E & Leahy RM Mapping human brain function with MEG and EEG: methods and validation. NeuroImage 23, S289–S299 (2004). [PubMed: 15501098]
79. Dannhauer M, Lanfer B, Wolters CH & Knösche TR Modeling of the human skull in EEG source analysis. Human Brain Mapping 32 (2011).
80. Wolters CH, et al. Influence of tissue conductivity anisotropy on EEG/MEG field and return current computation in a realistic head model: a simulation and visualization study using high-resolution finite element modeling. NeuroImage 30, 813–826 (2006). [PubMed: 16364662]
81. Cho JH, Vorwerk J, Wolters CH & Knösche TR Influence of the head model on EEG and MEG source connectivity analyses. Neuroimage 110, 60–77 (2015). [PubMed: 25638756]

82. Buchner H, et al. Inverse localization of electric dipole current sources in finite element models of the human head. Electroencephalography Clinical Neurophysiology 102, 267–278 (1997). [PubMed: 9146486]
83. Wolters CH, Grasedyck L & Hackbusch W Efficient computation of lead field bases and influence matrix for the FEM-based EEG and MEG inverse problem. Inverse Problems 20, 1099–1116 (2004).
84. Lew S, Wolters CH, Dierkes T, Röer C & Macleod RS Accuracy and run-time comparison for different potential approaches and iterative solvers in finite element method based EEG source analysis. Applied Numerical Mathematics 59, 1970–1988 (2009). [PubMed: 20161462]
85. Singh AK, Okamoto M, Dan H, Jurcak V & Dan I Spatial registration of multichannel multi-subject fNIRS data to MNI space without MRI. Neuroimage 27, 842–851 (2005). [PubMed: 15979346]
86. Tzourio-Mazoyer N, et al. Automated anatomical labeling of activations in SPM using a macroscopic anatomical parcellation of the MNI MRI single-subject brain. Neuroimage 15, 273–289 (2002). [PubMed: 11771995]
87. Lancaster JL, et al. Automated Talairach Atlas labels for functional brain mapping. Human Brain Mapping 10, 120–131 (2000). [PubMed: 10912591]
88. Jiang H, Bahramisharif A, van Gerven MA & Jensen O Measuring directionality between neuronal oscillations of different frequencies. Neuroimage 118, 359–367 (2015). [PubMed: 26025291]
89. Gross J, et al. Dynamic imaging of coherent sources: Studying neural interactions in the human brain. Proceedings of the National Academy of Sciences of the USA 98, 694–699 (2001). [PubMed: 11209067]
90. Nolte G, et al. Robustly estimating the flow direction of information in complex physical systems. Physical Review Letters 100, 234101 (2008). [PubMed: 18643502]
91. Klimesch W EEG alpha and theta oscillations reflect cognitive and memory performance: a review and analysis. Brain Research Reviews 29, 169–195 (1999). [PubMed: 10209231]
92. Klimesch W Alpha-band oscillations, attention, and controlled access to stored information. Trends in Cognitive Sciences 16, 606–617 (2012). [PubMed: 23141428]
93. Maris E & Oostenveld R Nonparametric statistical testing of EEG- and MEG-data. Journal of Neuroscience Methods 164, 177–190 (2007). [PubMed: 17517438]
94. Nolte G, et al. Identifying true brain interaction from EEG data using the imaginary part of coherency. Clinical Neurophysiology 115, 2292–2307 (2004). [PubMed: 15351371]
95. Storey JD A direct approach to false discovery rates. Journal of the Royal Statistical Society, Series B 64, 479–498 (2002).
96. Gazzaley A, Cooney JW, Rissman J & D'Esposito M Top-down suppression deficit underlies working memory impairment in normal aging. Nature Neuroscience 8, 1298–1300 (2005). [PubMed: 16158065]
97. McNab F, et al. Age-related changes in working memory and the ability to ignore distraction. Proceedings of the National Academy of Sciences 112, 6515–6518 (2015).
98. Chadick JZ, Zanto TP & Gazzaley A Structural and functional differences in medial prefrontal cortex underlie distractibility and suppression deficits in ageing. Nature Communications 5, 4223 (2014).

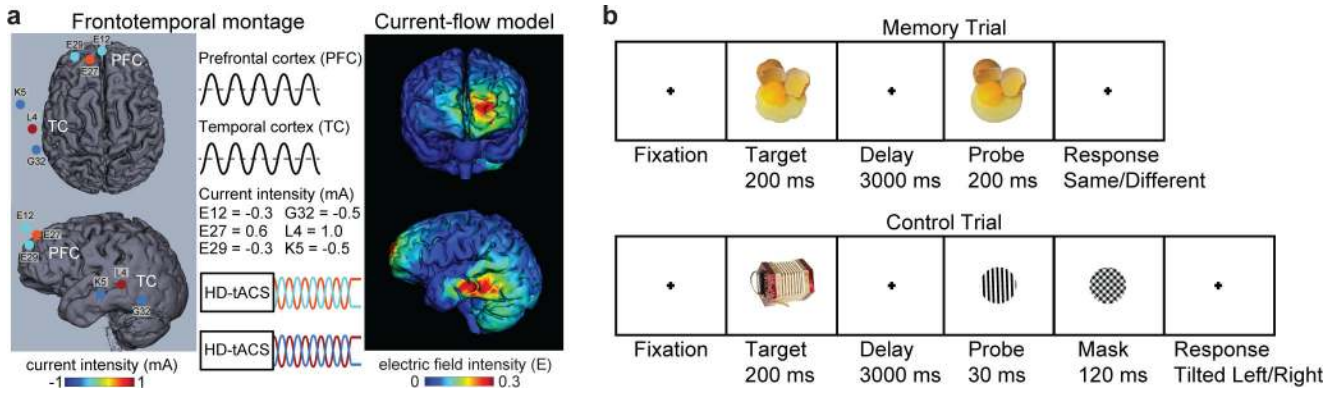

Fig. 1: Experiment 1, frontotemporal HD-tACS procedure and task.

a, The multifocal inphase frontotemporal HD-tACS montage and current-flow model shown on 3D reconstructions of the cortical surface. The location and current intensity value of each stimulating electrode are shown. The left prefrontal cortex and left temporal cortex were targeted, each with three electrodes in a center-surround, source-sink pattern to achieve maximum focality. **b**, All trials began with fixation followed by a target and then a delay period. In memory blocks, subjects judged whether a later probe was the same or a modified version of the target. In control blocks, subjects judged whether a backward masked grating probe was tilted clockwise or counterclockwise from the vertical and were not required to remember the target. Trial-by-trial adjustments in orientation magnitude of the probe ensured comparable performance across memory and control blocks.

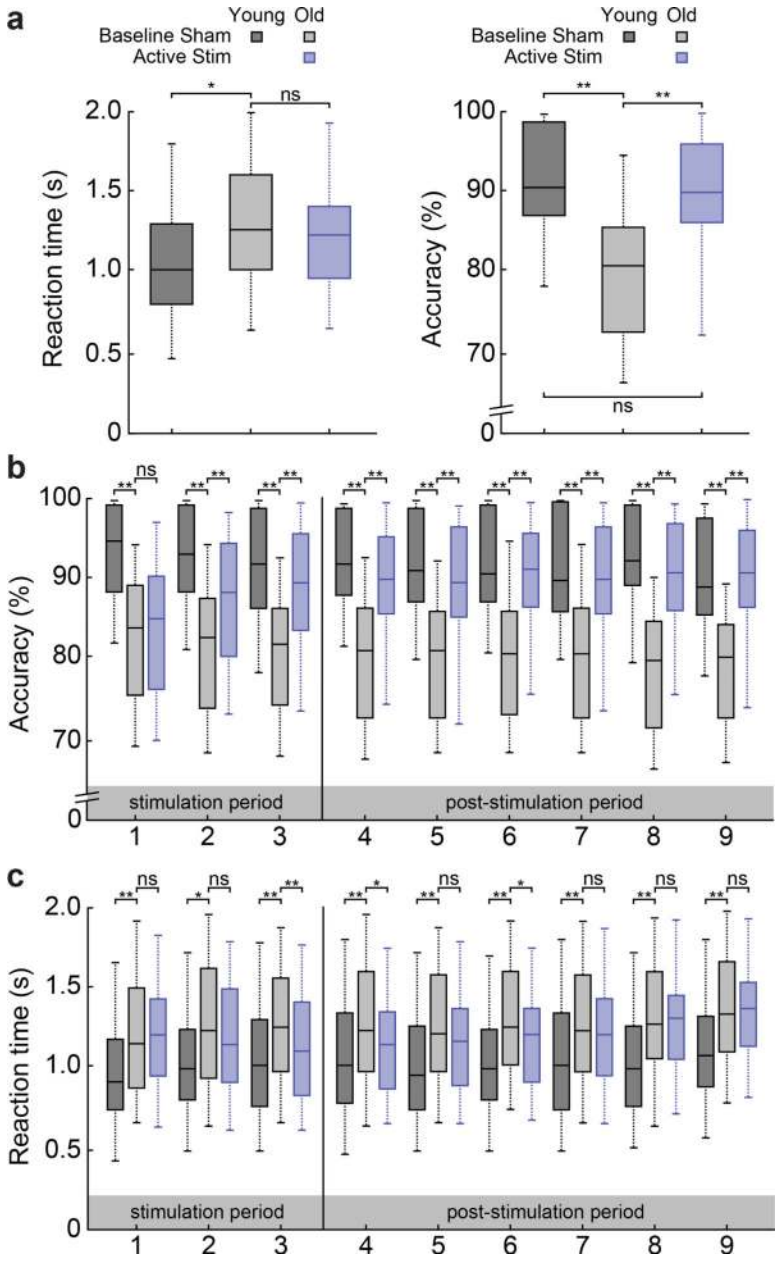

Fig. 2: Experiment 1, behavioral results.

a, Box plots of reaction time (RT) from correct trials and accuracy in post-stimulation memory blocks show older adults were slower ($t_{82} = 2.331$, $p = 0.022$, $d_z = 0.509$) and less accurate ($t_{82} = 5.587$, $p < 0.01$, $d_z = 1.219$) at baseline, relative to younger adults. After stimulation, accuracy improved ($t_{41} = 3.738$, $p = 0.001$, $d_z = 0.577$), removing the difference between groups ($t_{82} = 0.939$, $p = 0.350$, $d_z = 0.205$). RT did not differ between conditions ($t_{41} = 0.641$, $p = 0.527$, $d_z = 0.099$). Box plots of accuracy (**b**) and RT (**c**) from memory blocks sorted into 9 sequential bins (4 minutes per bin with 4 minutes between each bin from interleaved control blocks) shows significant group differences at every time bin for accuracy ($ts_{82} > 6.824$, $ps < 0.01$, $ds_z > 1.489$) and RT ($ts_{82} > 2.432$, $ps < 0.018$, $ds_z > 0.531$), at baseline. Stimulation improved accuracy at every time bin ($ts_{41} > 4.393$, $ps < 0.01$,

$ds_z > 0.678$), relative to sham, except the first ($t_{41} = 0.986$, $p = 0.330$, $d_z = 0.152$). Stimulation briefly sped RT at time bins 3 ($t_{41} = 2.841$, $p = 0.007$, $d_z = 0.438$), 4 ($t_{41} = 2.278$, $p = 0.028$, $d_z = 0.352$), and 6 ($t_{41} = 2.282$, $p = 0.028$, $d_z = 0.352$). Between-group comparisons used independent samples two-tailed *t*-tests ($n = 84$). Within-group comparisons used paired sample two-tailed *t*-tests ($n = 42$). Box-plot center, median; box limits, lower and upper quartiles; whiskers, lower and upper extreme values. * $p < 0.05$. ** $p < 0.01$.

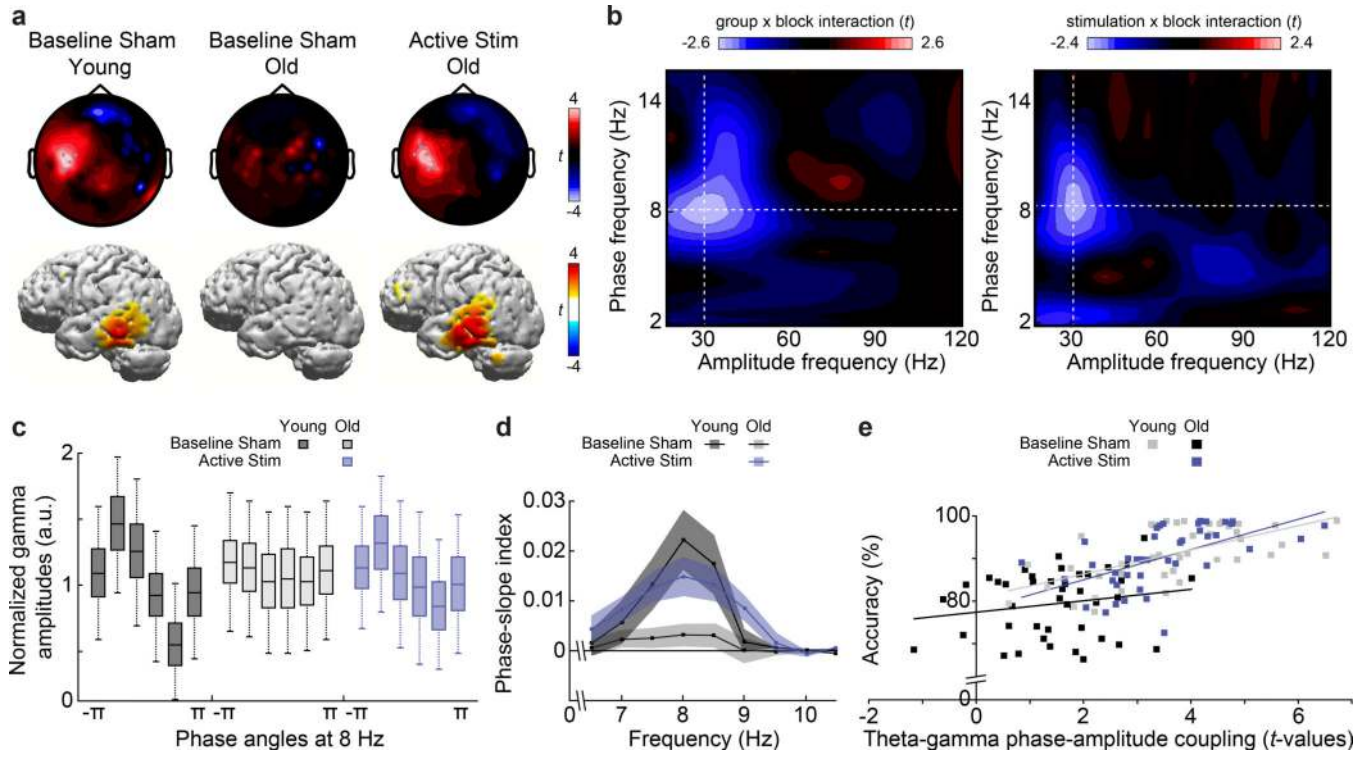

Fig. 3: Experiment 1, phase-amplitude coupling results.

a, Results show a significantly increased phase-amplitude coupling (PAC) cluster in left temporal electrodes (top) and voxels (bottom) for theta (7–9 Hz) phase and gamma (26–34 Hz) amplitude frequencies on memory compared to control blocks in younger adults at baseline and older adults after frontotemporal inphase theta HD-tACS ($p_{corrected} < 0.01$, two-sided cluster permutation test, $n = 42$). No other clusters were identified. **b**, Comodulograms show group x block and stimulation x block interactions for all combinations of low-frequency phase (2–16 Hz) and high-frequency amplitude (18–120 Hz) from left temporal electrodes showing significant PAC. Crosshairs indicate values where $t > -2.6$ or -2.4, respectively ($p_{corrected} < 0.01$, two-sided permutation test, $n = 42$). **c**, Box plots of gamma (26–34 Hz) amplitude binned by 8-Hz phase shown across groups and conditions ($n = 42$). **d**, Cross-frequency directionality between 6.5–10.5-Hz phase and 26–34-Hz amplitude from left temporal electrodes for each group and condition (center, mean; shaded region, SEM; $n = 42$). **e**, Individual subject Pearson correlations (two-tailed) between accuracy and theta-gamma PAC from left temporal electrodes for each group and condition ($n = 42$). Box-plot center, median; box limits, lower and upper quartiles; whiskers, lower and upper extreme values; points, outliers.

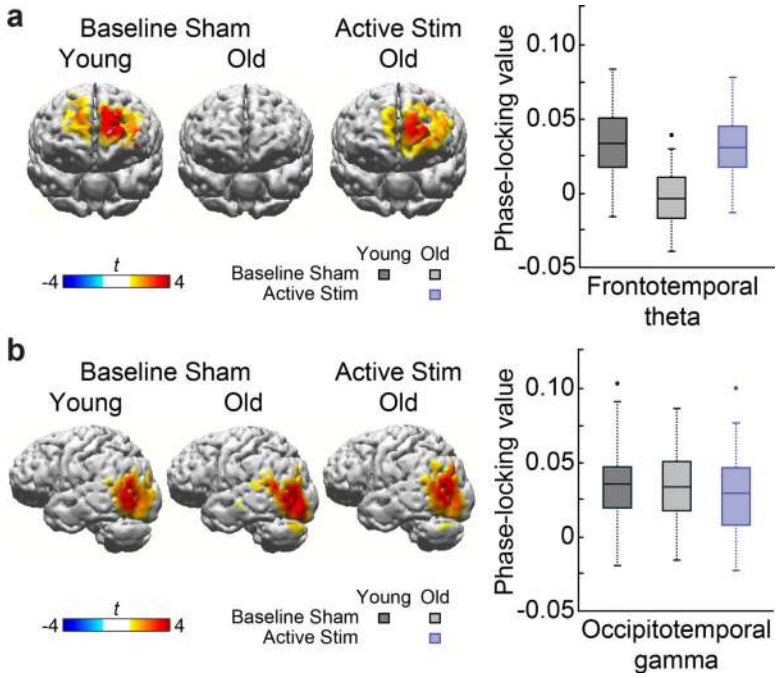

Fig. 4: Experiment 1, phase synchronization results.

a, A significant cluster in prefrontal cortex showed increased phase-locked value (PLV) with temporal cortex seed region in the theta band for younger adults at baseline and for older adults after stimulation ($p_{corrected} < 0.01$, two-sided cluster permutation test, $n = 42$). For theta PLV, the between-group difference at baseline ($t_{82} = 6.450$, $p < 0.01$, $d_z = 0.995$) and the between-condition difference within older adults ($t_{41} = 8.238$, $p < 0.01$, $d_z = 1.271$) were significant. **b**, A significant cluster in lateral occipital cortex showed increased PLV with temporal cortex seed region in the gamma band for each group and condition ($p_{corrected} < 0.01$, two-sided cluster permutation test, $n = 42$). For gamma PLV, there were no significant group ($t_{82} = 0.898$, $p = 0.374$, $d_z = 0.139$) or condition differences ($t_{41} = 1.012$, $p = 0.317$, $d_z = 0.156$). No other clusters were found. Between-group comparisons used independent two-tailed t-tests ($n = 84$). Within-group comparisons used paired sample two-tailed t-tests ($n = 42$). Box-plot center, median; box limits, lower and upper quartiles; whiskers, lower and upper extreme values; points, outliers.

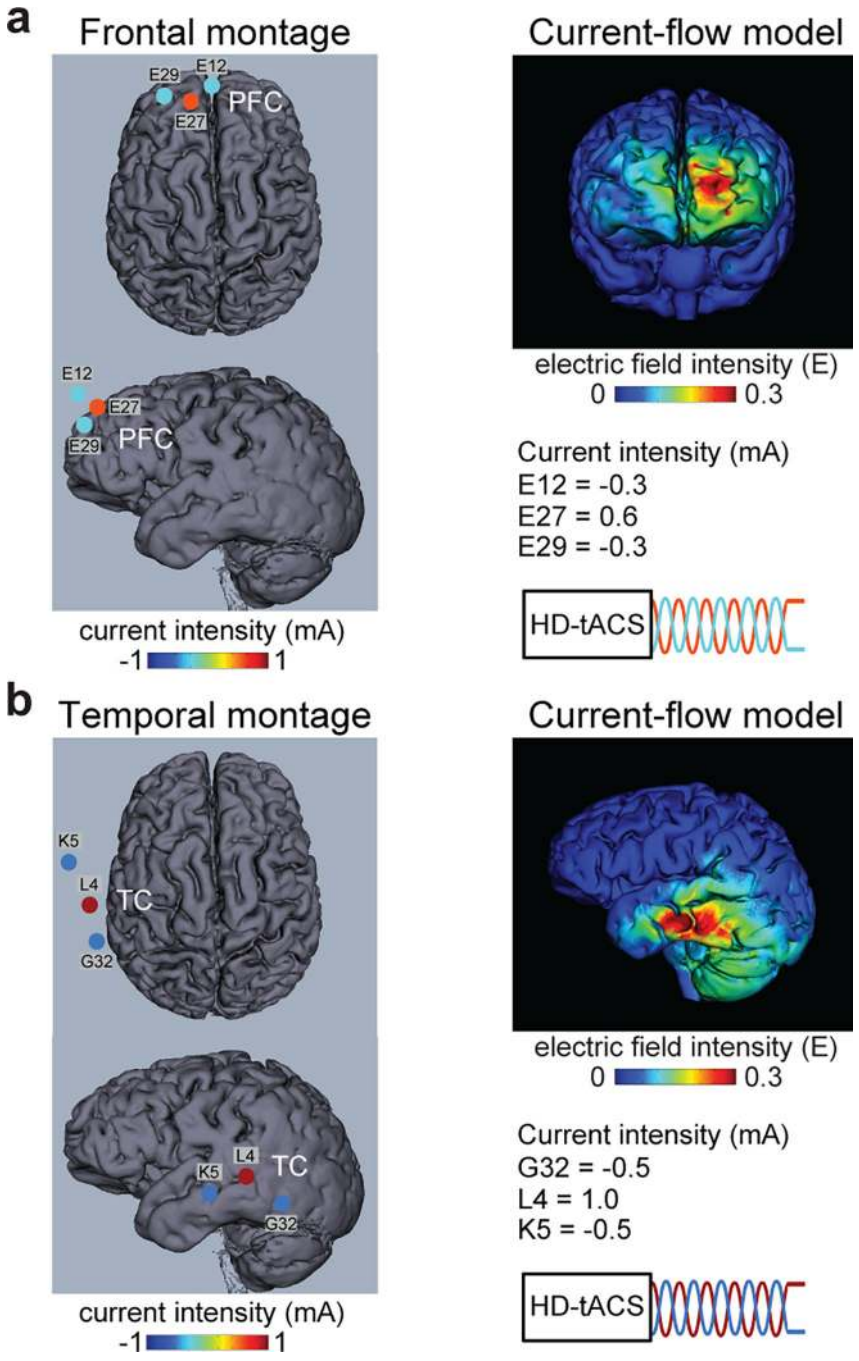

Fig. 5: Experiment 2, single-region HD-tACS procedures.

The unifocal frontal (**a**) and unifocal temporal (**b**) HD-tACS montages and current-flow models shown on 3D reconstructions of the cortical surface. The location and current intensity value of each stimulating electrode are shown. The frontal montage targeted left prefrontal cortex. The temporal montage targeted left temporal cortex. Each stimulation site used three electrodes in a center-surround, source-sink pattern to achieve maximum focality.

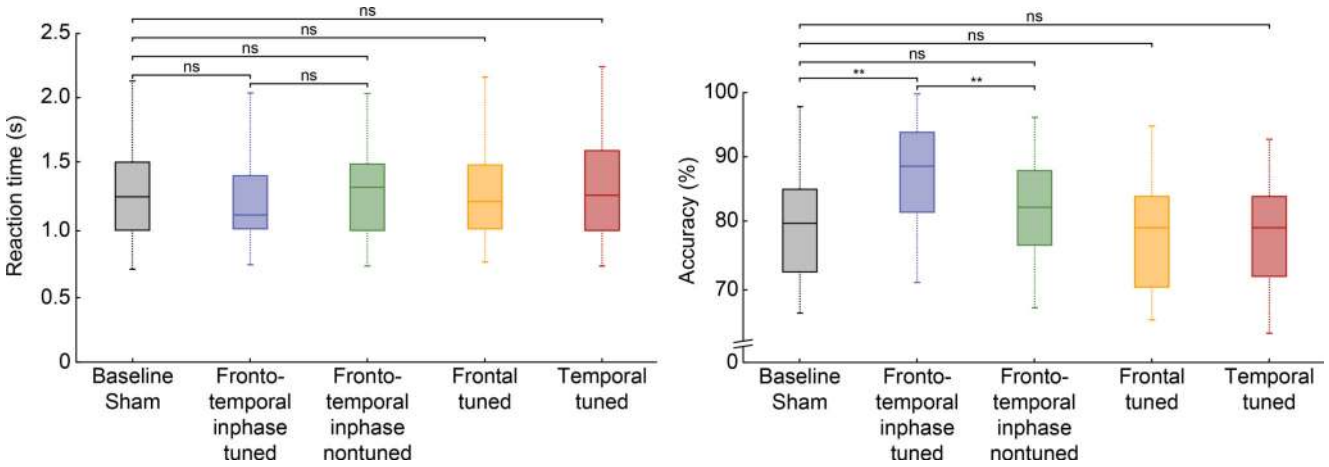

Fig. 6: Experiment 2, behavioral results.

Box plots of reaction time (RT) from correct trials and accuracy of older adults from post-stimulation memory blocks shown across the stimulation conditions of Experiment 2. Relative to sham, frontotemporal inphase theta-tuned stimulation exerted a preferential improvement in task accuracy ($t_{27} = 3.101$, $p = 0.004$, $d_z = 0.586$) without changing RT ($t_{27} = 1.278$, $p = 0.212$, $d_z = 0.242$). Nontuned stimulation had no significant impact on accuracy ($t_{27} = 1.211$, $p = 0.236$, $d_z = 0.229$), or RT ($t_{27} = 0.406$, $p = 0.688$, $d_z = 0.077$), relative to sham. Frontal-alone and temporal-alone stimulation had no significant effect on RT (frontal, $t_{27} = 0.182$, $p = 0.857$, $d_z = 0.034$; temporal, $t_{27} = 0.085$, $p = 0.933$, $d_z = 0.016$) or accuracy (frontal, $t_{27} = 0.323$, $p = 0.749$, $d_z = 0.061$; temporal, $t_{27} = 0.162$, $p = 0.873$, $d_z = 0.031$). Paired sample two-tailed *t*-tests ($n = 28$). Box-plot center, median; box limits, lower and upper quartiles; whiskers, lower and upper extreme values. ** $p < 0.01$.